energies

MDPI

Article

Study of the Failure Mechanism of an Integrated Injection-Production String in Thermal Recovery Wells for Heavy Oil

Wei Zhang [1], Deli Gao [1,*], Yigang Liu [2], Jianhua Bai [2] and Cheng Wang [2]

[1] College of Petroleum Engineering, China University of Petroleum-Beijing, Beijing 102249, China
[2] China National Offshore Oil Corporation China Ltd., Tianjin Branch, Tianjin 300459, China
* Correspondence: gaodeli@cup.edu.cn

Abstract: The integrated injection-production string is the core tool used in thermal recovery wells for heavy oil, the mechanical behavior of which is complex due to the coupling effect of downhole temperature and pressure and the load induced by steam huff and puff operations. In this paper, an analysis model that calculates the temperature and pressure field during steam huff and puff operations has been established based on the basic principles of energy conservation and heat transfer. Then, the force distribution and strength check of the integrated injection-production string were analyzed. The fatigue damage of the string was evaluated by considering dynamic loads during the injection process. The corrosion life of the string was predicted. Finally, the failure mechanism of the integrated injection-production string in thermal recovery wells for heavy oil was illustrated. The results showed that the strength of the string and vibration fatigue are not the main causes of failure, but corrosion is the main reason for string failure. The residual strength of the corroded string was greatly reduced, which is the fundamental reason for the failure of the string. This paper is of guiding significance to the optimization of design and safety evaluations of the integrated injection-production string in thermal recovery wells for heavy oil.

Keywords: heavy oil; thermal recovery well; integrated injection-production string; downhole tubular mechanics; failure mechanism

check for updates

Citation: Zhang, W.; Gao, D.; Liu, Y.; Bai, J.; Wang, C. Study of the Failure Mechanism of an Integrated Injection-Production String in Thermal Recovery Wells for Heavy Oil. *Energies* **2023**, *16*, 3246. https://doi.org/10.3390/en16073246

Academic Editor: Xinpu Shen

Received: 6 March 2023
Revised: 27 March 2023
Accepted: 30 March 2023
Published: 5 April 2023

Copyright: © 2023 by the authors. Licensee MDPI, Basel, Switzerland. This article is an open access article distributed under the terms and conditions of the Creative Commons Attribution (CC BY) license (https://creativecommons.org/licenses/by/4.0/).

1. Introduction

Currently, steam "huff and puff" technology has become the most commonly used method for heavy oil reservoir exploitation due to its efficiency and flexibility, which is achieved by injecting a large amount of high dry steam into a reservoir through an integrated injection-production string. After a period, the viscosity of the heavy oil will be greatly reduced, and the fluidity will be increased [1–3]. When compared with conventional oil production, the integrated injection-production string is the main tool of steam injection, which is subjected to high temperatures and high pressures (HTHPs) for long periods. Besides, the operating load induced by the injection and production is also complex, which frequently causes the failure of the string. Therefore, it is important to ensure the safety of the string by analyzing the mechanical characteristics and revealing the failure mechanism.

So far, some scholars have carried out research on the mechanical behavior of the integrated injection-production string. Cullender et al. [4] have obtained the well pressure distribution under steady-state flow conditions by using average temperature and deviation coefficients. Ramey [5] has analyzed the temperature through regarding the incompressible liquid temperature and single-phase as a function of well depth and time. Wang [6] has established the semi-analytical method of heat transfer and calculated the well temperature through unsteady heat transfer. Mao et al. [7] have developed a coupled temperature-pressure analysis model by considering the interaction operation. Zhang et al. [8] have derived the iterative formula for the calculation of well pressure by using

the average method. Shi et al. [9] established a coupled prediction model for temperature and pressure distribution based on the conservation of momentum and energy and the basic principles of mass and heat transfer. Cao et al. [10,11] proposed a model of temperature profile variation in the production string by taking into account the influence of flow friction and gas properties. Under the coupling effect of temperature and pressure, a variety of mechanical effects will be generated in the integrated injection-production string. Therefore, some scholars have conducted relevant studies on the mechanics of the string. Johancsik et al. [12] established the drag-torque model of a downhole string, which simplified the string into a rope without bending stiffness. Mitchell et al. [13] proposed a rigid rod model by considering the contact position between the string and borehole. Mayouf et al. [14] proposed a method for calculating the large deformation and torque of a string based on the beam theory. Wang et al. [15] established a stress analysis model of the test string of HTHPs in gas wells. A dynamic load will be induced in the HTHP steam injection and production process, which will cause alternating stress and, eventually, fatigue damage in the string. Therefore, some scholars have conducted studies on the dynamic mechanical behavior and fatigue damage of strings under HTHP conditions. C Semler et al. [16] established the nonlinear differential equation of a liquid-filled string by considering the influence of a large curvature and transverse deflection. Ding [17] conducted simulation experiments to study the vibration of a gas production string, which found that the vibration of the string is related to the flow rate and velocity of the gas. In terms of fatigue analysis, Manson et al. [18] obtained the Manson–Coffin equation through a large number of experimental studies and established the bilinear fatigue cumulative damage theory. Neuber [19] studied the fatigue life through the local stresses method and proposed the Neuber criterion. Based on a large number of experimental studies on fatigue damage, Miner formalized the linear cumulative damage theory proposed by Palmgren and established the Palmgren–Miner linear cumulative damage criterion, which has become one of the commonly used methods for a fatigue damage assessment at present [20]. Liu et al. [21] reviewed the application of the rain flow counting method for fatigue damage evaluation. Liu et al. [22] predicted the fatigue life of an HTHP string by combining the S-N curve and linear cumulative damage theory. Song et al. [23] analyzed the internal pressure strength of the corroded casing. Sun et al. [24] calculated the stress concentration coefficient of a spherical pit in the corroded casing. JW et al. [25] calculated a strength check using the finite element analysis method. Mu et al. [26] analyzed the relationship between strength and corrosion depth and established a formula for calculating the service life of a casing string. Yuan [27] obtained the residual extrusion and compressive strength of a casing according to API-recommended practice. Xu et al. [28] analyzed the residual internal pressure and extrusion strength of a casing after corrosion by using elastic-plastic theory.

At present, great progress has been achieved in the mechanical behavior analysis of HPHT strings as well. However, the structural composition of an integrated injection-production string in thermal recovery wells is complex. In addition, string failures caused by temperature, pressure, and external loads occur from time to time. Therefore, it is necessary to study the mechanical behavior of the string and reveal its failure mechanism. For this purpose, the temperature and pressure field, the mechanical vibration properties, and the strength check and corrosion life of the integrated injection-production string were studied. Finally, the failure mechanism of the string has been clarified. This study is of guiding significance to the design and control of integrated injection-production strings.

2. Mechanical Analysis

2.1. Temperature and Pressure

The composition of an integrated injection-production string in a thermal recovery well for heavy oil is shown in Figure 1. As shown in Figure 1, the string mainly includes a thermal insulation string, a high-temperature-resistant packer, a jet pump barrel, a blowout preventer valve, a Y-type crossing device, a high-temperature thermal recovery packer, and a top packer.

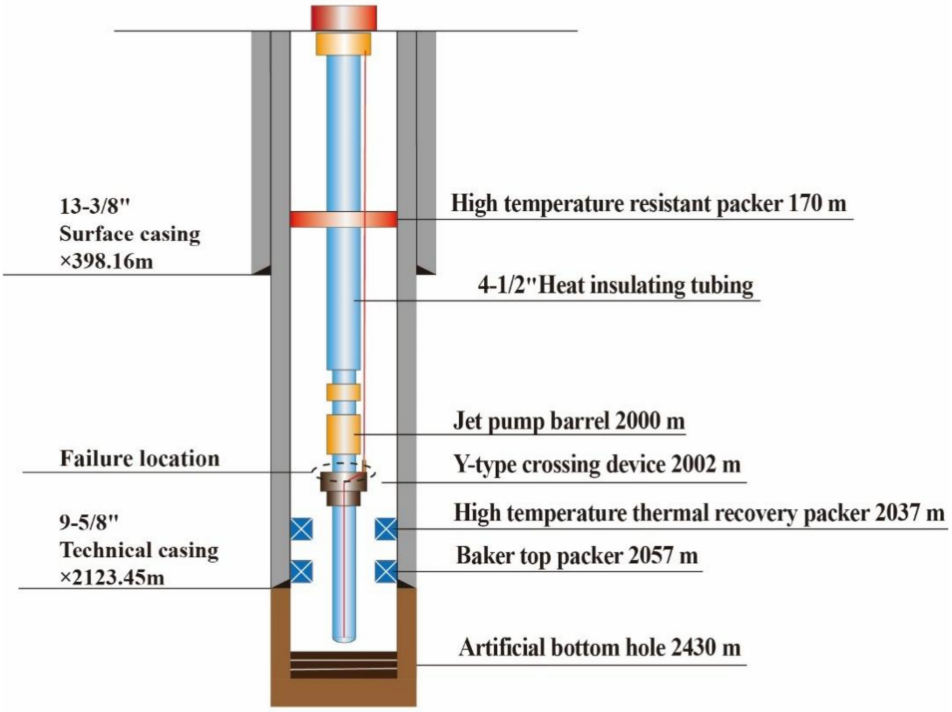


Figure 1. Schematic diagram of integrated injection-production string.

In order to simplify the mathematical derivation, the following assumptions are adopted in the analysis:

1. The fluid flow in the wellbore is regarded as stable flow, and all parameters of the fluid in the same plane are the same.
2. The heat transfer in the axial direction is in a stable state, while the heat transfer in the radial direction is in a transient state.

The constructed co-ordinate system is shown in Figure 2. Take a segment of the microelement as the object of study: the length of the microelement is dx. The flow, pressure, and rate at dx are p, Q, and v, while the above parameters at $x + dx$ are $p + dp$ are $Q + dQ$ and $v + dv$, respectively.

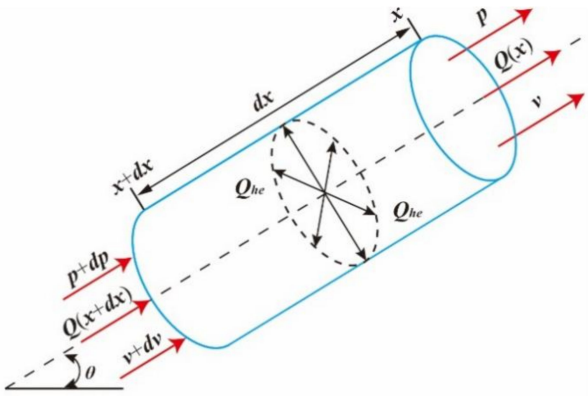


Figure 2. Analysis model of temperature and pressure.

According to the energy conservation and momentum theory [9], one obtains:

$$\begin{cases} w\left(\frac{dH}{dx} + \frac{vdv}{dx} + gsin\,\theta - f\frac{v^2}{2d}\right) + Q = 0 \\ \frac{dp}{dx} = -\rho v\frac{dv}{dx} - \rho g\sin\theta - f\frac{\rho v^2}{2d} \end{cases} \quad (1)$$

where ρ is the fluid density, kg/m^3; ν is the fluid velocity, m/s; x is the well depth, m; p is pressure, Pa; g is the acceleration of gravity, m/s^2; θ is the angle between the axial direction and the horizontal direction of the string, (°); f is the friction coefficient, dimensionless; d is the inner diameter of the string, m; w is the mass flow rate of fluid, kg/s; H is the specific enthalpy, J/kg; Q_{he} is the heat loss per unit length, J/(m·s).

The enthalpy change equation [29] can be expressed as

$$\frac{dH}{dx} = c_p \frac{dT}{dx} - c_p c_J \frac{dp}{dx} \tag{2}$$

The heat loss of gas during flow can be expressed as [30]:

$$Q_{he} = w c_p (T - T_{ei}) L_R \tag{3}$$

where T_{ei} is the original formation temperature, K; T is the fluid temperature of the insulated string, K; c_p is the specific heat capacity of the fluid, J/(kg·K); L_R is the relaxation distance parameter, $L_R = \frac{2\pi}{w c_p}\left(\frac{r_{to} U_{to} K_e}{K_e + r_{to} U_{to} T_D}\right)$; K_e is the formation thermal conductivity, W/(m·K); r_{to} is the outer radius of the string, m; U_{to} is the total heat transfer coefficient, J/(s·m^2·K); T_D is a dimensionless time function; c_J is the Joule-Thompson coefficient, MPa/K; p is the pressure in the string, MPa.

$$\begin{cases} \frac{dp}{dx} = \frac{\rho g sin\,\theta + f\frac{\rho v^2}{2d}}{(\rho v^2/p - 1)} \\ c_p \frac{dT}{dx} = -\frac{2\pi r_{t0} U_{T0} K_e}{W[r_{t0} U_{T0} f(t) + K_e]}(T - T_{ei0} + g_G z \sin\theta) + c_p c_J \frac{dP}{dx} + \frac{v^2}{p}\frac{dP}{dx} + f\frac{v^2}{2d} - g sin\,\theta \end{cases} \tag{4}$$

where, e$T_{ei} = T_{ei0} - g_G z \sin\theta$, $\phi = g_G sin\,\theta + \psi - \frac{g \sin\theta}{c_p}$ and $\psi = -c_J \frac{dP}{dz} + \frac{\nu}{c_p}\frac{dv}{dz}$; g_G is the geothermal gradient, K/m.

2.2. Stress and Deformation

2.2.1. Basic Effects

During the gas injection process, the following three effects will occur due to the influence of the coupling effect of temperature and pressure.

1. Piston effect

The axial force of the string will change suddenly due to the change of cross-sectional area, which will cause the piston effect, as shown in Figure 3.

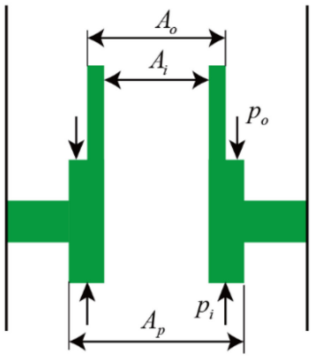


Figure 3. Schematic diagram of piston effect.

As shown in Figure 3, the axial force F_1 acting on the string induced by the piston effect can be expressed as [31]

$$F_1 = p_o(A_p - A_o) - p_i(A_p - A_i) \tag{5}$$

where p_o is the external pressure, Pa; p_i is the internal pressure, Pa; A_p is the external cross-sectional area of the packer, m^2; A_i is the cross-sectional area of the string, m^2; A_o is the cross-sectional area outside the string, m^2.

The axial deformation of the string caused by piston effect ΔL_1 can be expressed as [31]

$$\Delta L_1 = \frac{L}{EA_{tc}}\left[\Delta p_o\left(A_p - A_o\right) - \Delta p_i\left(A_p - A_i\right)\right] \tag{6}$$

where L is the total length of the string, m; E is the elastic modulus; Pa; A_{tc} is the cross-sectional area of the string, m^2.

2. Expansion effect

During gas injection, the gas pressure inside and outside the heat-insulation string is different, which will cause an expansion effect and lead to radial expansion or compression of the string insulated, as shown in Figure 4a, the pressure acting on the wall of the tubing will reduce the diameter of the tubing string, when the external pressure is greater than the internal pressure. Conversely, if the internal pressure is greater than the external pressure, the diameter of the tubing string will increase in Figure 4b.

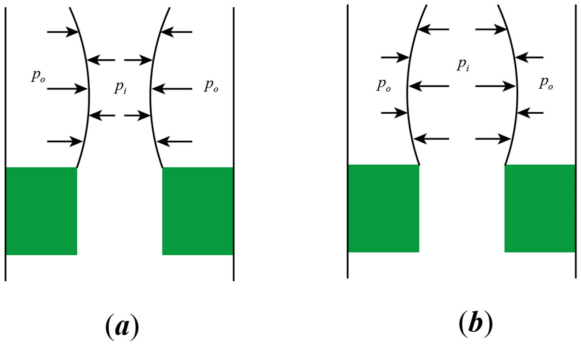


Figure 4. Diagram of the expansion effect.

If the external pressure of the string above the packer is greater than the internal pressure, the radial diameter of the string will decrease, and the string length will increase, as shown in Figure 4a. Conversely, the radial diameter of the string will increase, and the string length will shorten, as shown in Figure 4b.

According to the theory of elasticity, the axial deformation caused by the expansion effect of the string ΔL_2 can be expressed as [32]

$$\Delta L_2 = -\frac{\mu}{E}\frac{\Delta\rho_i - R^2\Delta\rho_o - \delta\frac{1+2\mu}{2\mu}}{\xi^2 - 1}L^2 - \frac{2\mu}{E}\frac{\Delta p_i - R^2\Delta p_o}{\xi^2 - 1}L \tag{7}$$

where μ is the Poisson's ratio, dimensionless; $\Delta\rho_i$ is the change of gas density in the string, kg/m^3; $\Delta\rho_o$ is the change of gas density outside the string, kg/m^3; ξ is the ratio between the outer diameter and the inner diameter of the string, non-dimensional; δ is the pressure drop per unit length of the string, Pa/m; Δp_i is the internal pressure change, Pa; Δp_o is the change of the external pressure, Pa.

Therefore, the axial force F_2 of the string caused by the expansion effect can be expressed as [32]:

$$F_2 = 2\mu A_{tc}\frac{\xi^2\Delta\rho_o - \Delta p_i}{R^2 - 1} \tag{8}$$

3. Temperature effect

Due to the temperature difference between the formation and the string, the temperature of the string will change until it reaches the equilibrium, which is called the

temperature effect. The axial deformation of the string caused by temperature effect ΔL_3 can be expressed as [32]

$$\Delta L_3 = \beta L(T_i - T_o) \tag{9}$$

where β is the thermal expansion coefficient, $1/^\circ$C; T_i is the average temperature of the string, °C; T_o is the formation temperature, °C.

Therefore, the axial force F_3 acting on the string due to the temperature effect can be expressed as [33]

$$F_3 = E\beta A_{tc}(T_i - T_o) \tag{10}$$

2.2.2. Strength Check

In this paper, the following assumptions are adopted during the mechanical behavior and strength check.

(1) The cross-sectional area of the string is a circle;
(2) The axis of the string is the same as the axis of the well;
(3) The internal pressure, external pressure, and friction resistance of the string are distributed uniformly.

According to the above assumptions, the mechanical model of axial stress and deformation of the string is shown in Figure 5.

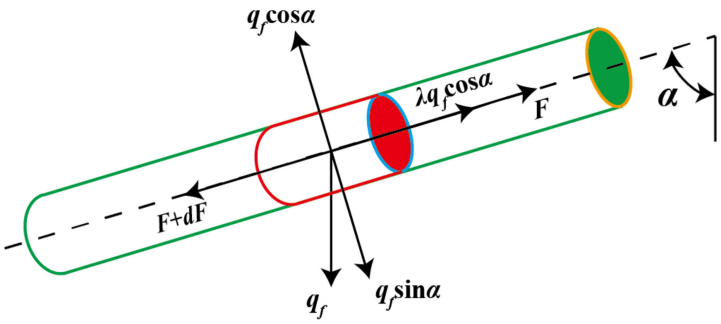


Figure 5. Mechanical model of the string.

The governing equation of the mechanical behavior can be written as [9]

$$\frac{\partial^2 u}{\partial s^2} = K_B \frac{\lambda\rho g\sin\alpha - \rho g\cos\alpha}{E} \tag{11}$$

The initial conditions and boundary conditions of Equation (11) can be expressed as

$$\begin{cases} u(0) = 0 \\ EA_{tc}\frac{\partial u}{\partial s}(L) = -F_s \end{cases} \tag{12}$$

where u is the axial displacement, m; K_B is the buoyancy coefficient, dimensionless; λ is the friction coefficient which is 0.25 in this paper; α is the well inclination angle, (°); F_s is the setting force of the packer, N.

Combined Equations (11) and (12), the axial deformation of the string can be obtained. Then, according to Equation (13), the axial force caused by the axial deformation can be obtained, which is

$$F_s = EA_{tc}\frac{\partial u}{\partial s} \tag{13}$$

Therefore, the total axial force F_a on the string can be expressed as [33]

$$F_a = F_1 + F_2 + F_3 + F_s \tag{14}$$

Considering the bending moment, the maximum axial stress σ_a on the outer wall of the string can be expressed as

$$\sigma_a = \frac{F_a}{A_{tc}} + \frac{2\pi E A_{tc} r_{to} \varnothing}{L_i} \tag{15}$$

where r_{to} is the outer diameter of the string, m; $\varnothing$ is the dogleg angle of the well hole, °/30 m; L_i is the length of the string, m.

According to elastic theory, the strength check of the string can be expressed as [33]

$$\sigma_s = \frac{\sqrt{2}}{2}\sqrt{(\sigma_a - \sigma_\theta)^2 + (\sigma_\theta - \sigma_r)^2 + (\sigma_r - \sigma_a)^2} \le \frac{\left[\sigma_{yield}\right]}{n} \tag{16}$$

where σ_r and σ_θ are the radial stress and circumferential stress which can be calculated by the Lamme equation of elasticity, MPa. $\left[\sigma_{yield}\right]$ is the yield strength of the string, MPa; n is the safety factor.

2.3. Fatigue Damage

During steam huff and puff operations, vibration will occur due to the influence of temperature difference, nonuniform internal and external pressure, axial force and nonuniform steam injection, and other factors, which will generate fatigue damage to the string.

Therefore, fatigue damage prediction of integrated injection and production string is of great significance to ensure the safe operation of the pipe string. In this paper, the finite element method is used to establish the physical model of the integrated injection-production string. The loads such as temperature, pressure, axial force, and gas injection condition are applied to the string to obtain the mechanical vibration response. Then, according to the finite element analysis results, the equivalent stress time history of the critical position is extracted. The stress time history is sorted out according to the rain-flow counting method [34,35], and the average stress is modified by the Goodman curve [36,37]. Finally, the fatigue damage is calculated by S-N curve and the Palmgren–Miner linear fatigue cumulative damage theory [36,37].

According to published results [38], the S-N curve of fatigue damage analysis can be expressed as

$$lgS = lgK - mlgN \tag{17}$$

where S is the stress value, MPa; N is the number of load cycles; lgK is -0.0585; m is 2.7202 in this paper.

The cumulative fatigue damage of the string is calculated by the Palmgren–Miner linear cumulative damage theory, where it is assumed that at any given stress level, the cumulative damage rate is independent of the previous loading process, and the loading order does not affect the calculated value of fatigue damage. The Palmgren–Miner linear cumulative damage calculation formula can be expressed as

$$\begin{cases} D_j = \sum\limits_{i=1}^{k} \frac{n_i}{N_i} \\ D = \sum\limits_{j=1}^{m} p_j D_j \end{cases} \tag{18}$$

where n_i is the actual cycle number of the load; N_i is the allowable cycle number of the load, and D_j is the fatigue damage of the string under a certain working condition; p_j is the proportion of the total working time of the certain condition; D is fatigue damage of the string under different working conditions.

2.4. Life Prediction after Corrosion

Corrosion can reduce the bearing capacity and shorten its service life significantly. Therefore, the service life prediction of a corroded string and the timely detection of string failure can avoid unnecessary economic losses.

The following assumptions were made during the modeling process in this paper.

1. The string is assumed to be thick-walled and under the three-dimensional stress state of internal pressure, external pressure, and axial tension;
2. The uniform corrosion occurs only on the inner wall of the string;
3. The mechanical action on the string only affects the corrosion rate of the string;
4. The circumferential stress on the inner wall of the string without corrosion can be obtained from Lamme's formula, which is

$$\sigma_{t0} = \frac{P_i r_i^2 - P_o r_o^2}{r_o^2 - r_i^2} + \frac{(P_i - P_o) r_i^2 r_o^2}{r_o^2 - r_i^2} \cdot \frac{1}{r_i^2} = \frac{P_i (r_i^2 + r_o^2) - 2P_o r_o^2}{r_o^2 - r_i^2} \tag{19}$$

where σ_{t0} is the circumferential stress, MPa; P_i is the internal pressure, MPa; P_o is the external pressure, MPa; r_i is the inner diameter, mm; r_o is the outer diameter, mm.

If the corrosion depth is h, the circumferential stress on the inner wall of the string is

$$\sigma_t = K\left[\frac{P_i (r_i + h)^2 - P_o r_o^2}{r_o^2 - (r_i + h)^2} + \frac{(P_i - P_o)(r_i + h)^2 r_o^2}{r_o^2 - (r_i + h)^2} \cdot \frac{1}{(r_i + h)^2}\right] = K \cdot \frac{P_i (r_i + h)^2 + P_i r_o^2 - 2P_o r_o^2}{r_o^2 - (r_i + h)^2} \tag{20}$$

where σ_t is the circumferential stress, MPa; h is the corrosion depth of the string, mm; K is the stress concentration coefficient.

Therefore, the change rate of the circumferential stress of the string is

$$\frac{d\sigma_t}{dt} = \frac{(\sigma_t + Kp_i)^{3/2}\sqrt{\sigma_t + K(2p_o - p_i)}}{Kr_{to}(p_i - p_o)} \frac{dh}{dt} \tag{21}$$

According to the published results, one obtains [39]

$$\frac{dh}{dt} = v_0 exp\left(\frac{V\sigma_t}{RT}\right) \tag{22}$$

where V is the molar volume of the string material, mm^3/mol; R is the general constant of gas, J/(mol·K); T is the absolute temperature, K; v_0 is the corrosion rate, mm/a.

Substituting Equation (22) into Equation (23), the corrosion life of the string can be written as

$$t_l = \frac{Kr_{to}(p_i - p_o)}{v_0} \int_{\sigma_{t0}}^{\sigma_{tf}} \frac{d\sigma_t}{(\sigma_t + Kp_i)^{3/2}\sqrt{\sigma_t + K(2p_o - p_i)} exp\left(\frac{V\sigma_t}{RT}\right)} \tag{23}$$

3. Case Study

3.1. Calculation Data

Taking Well X as an example to analyze the temperature and pressure distribution, the well structure is shown in Figure 6. From the results of the engineering site, it was found that the outer layer of the string had been disconnected from the lower part of the 4–1/2" string. The outer layer of the string broke at the body connection of the Y-shaped crossing device. Besides, it was found that serious corrosion occurred at the fracture of the string. After physical and chemical analysis, it was found that the main corrosion products were Fe_3O_4 and SiO_2 and a small amount of chlorine elements from the water. The preliminary judgment is that the corrosion of the string is caused by oxygen corrosion under the environment of high-temperature water steam. The other calculation parameters

of the well are shown in Table 1, and the chemical composition of the steel of the string is shown in Table 2.

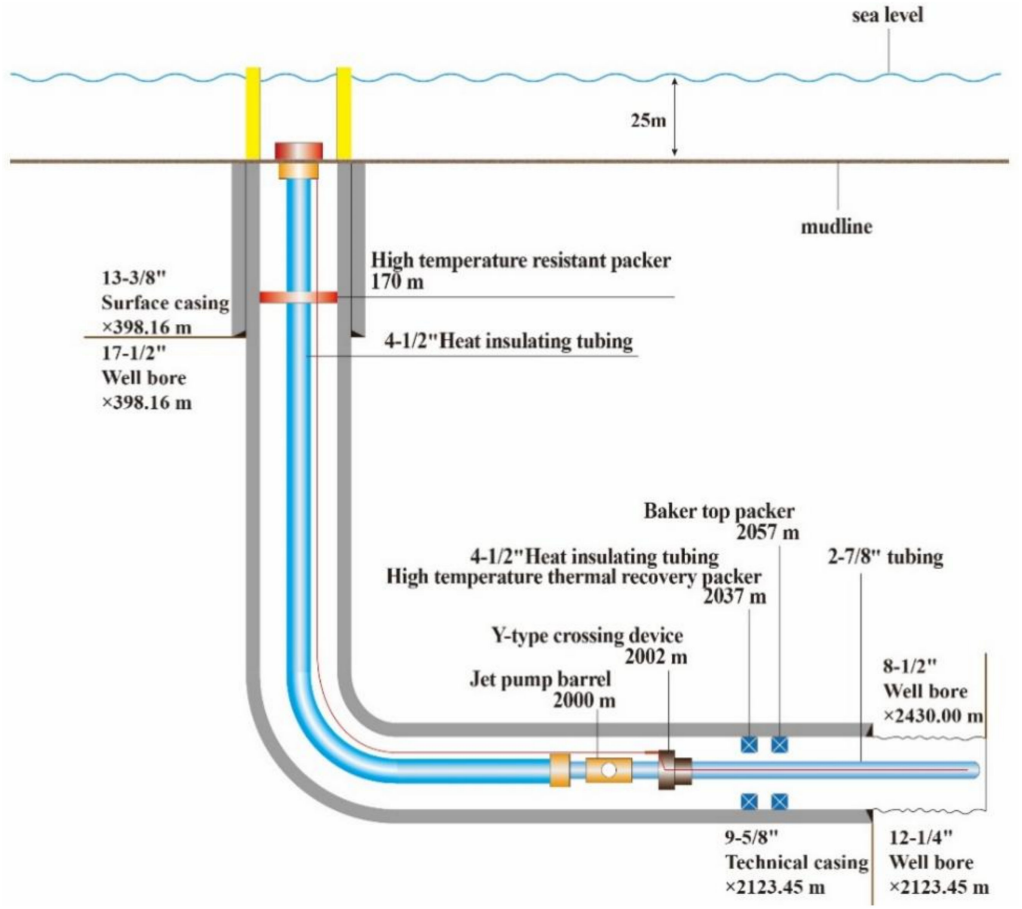


Figure 6. Well structure for Well X.

Table 1. Basic operating parameters.

Parameter	Value	Parameter	Value
Well Depth (m)	2430	Wellhead Pressure (MPa)	14.6
Formation Diffusion coefficient (m^2/s)	5.7×10^{-8}	Injection temperature (°C)	340
Outer Diameter of the String (m)	0.1143	Geothermal gradient (°C/100 m)	2.7
Inner Diameter of the String (m)	0.1005	Bottomhole Pressure (MPa)	1.65
Inner Diameter of Casing (m)	0.2237	Bottomhole Temperature (°C)	340
Formation Thermal Conductivity W/(m·°C)	1.74	Gas Injection Speed (m^3/d)	300
Gas-Liquid Ratio	51/1	Cement Thermal Conductivity W/(m·°C)	1.2
Corrosion Rate (mm/a)	0.15	Molar Volume (mm^3/mol)	7

Table 2. The chemical composition of the string material.

Element	w/%	Element	w/%
C	0.290	Si	0.240
Mn	1.310	P	0.014
S	0.003	Ni	0.030
Cr	0.100	Cu	0.060
Mo	0.010	Fe	-

3.2. Results

3.2.1. Model Verification

In order to verify the correctness of the mathematical model and solution method established in this study, model validation was conducted. Table 3 shows the parameters for the model validation [6].

Table 3. Calculation data for model validation.

Parameter	Value	Parameter	Value
Well Depth (m)	4500	Bottom Hole Pressure (MPa)	57.3
Bottom Hole Formation Temperature (°C)	123.4	Gas Production (m^3/d)	50×10^4
outer diameter of tubing (mm)	88.9	Thermal Diffusion Coefficient of Formation (m^2/s)	1.21×10^{-6}
Inner Diameter of Tubing (mm)	76.0		

As shown in Figure 7, temperature 1 and pressure 1 are the calculated results from the published results [6], and temperature 2 and pressure 2 are the results calculated by this work. The results calculated according to the model in this study are in good agreement with the published results, which indicates the accuracy of the model and solution method established in this study.

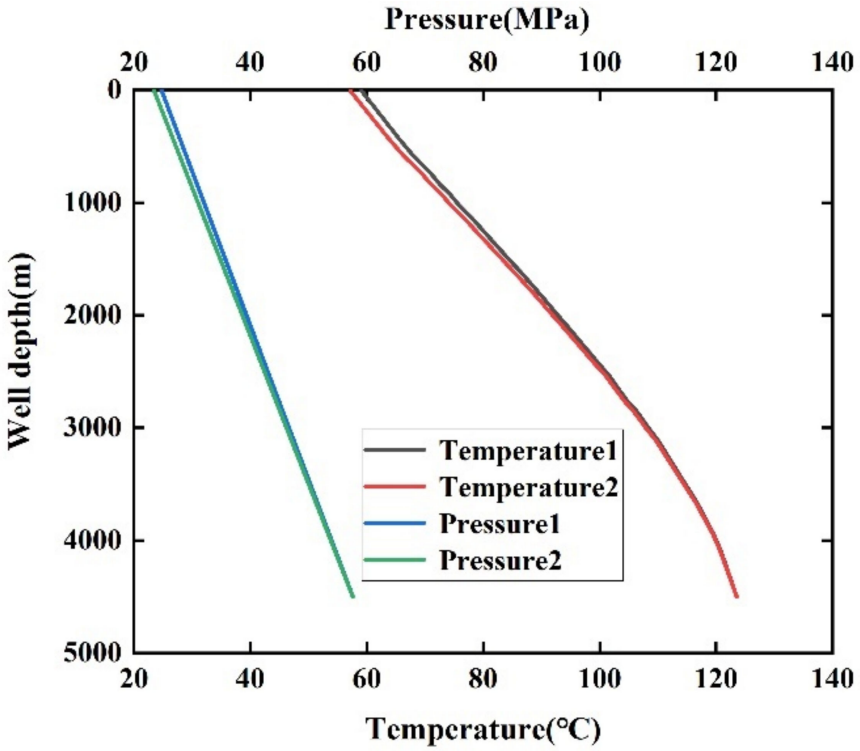


Figure 7. Model verification results.

3.2.2. Temperature and Pressure Distribution

According to the analysis model established in this paper, the temperature and pressure distribution of the whole well section is shown in Figures 8 and 9.

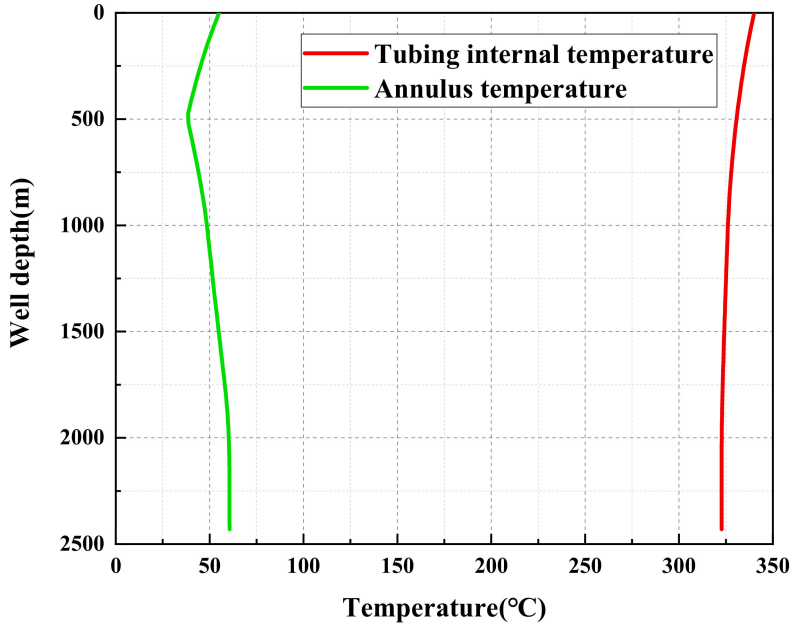


Figure 8. Temperature distribution of the integrated injection-production string.

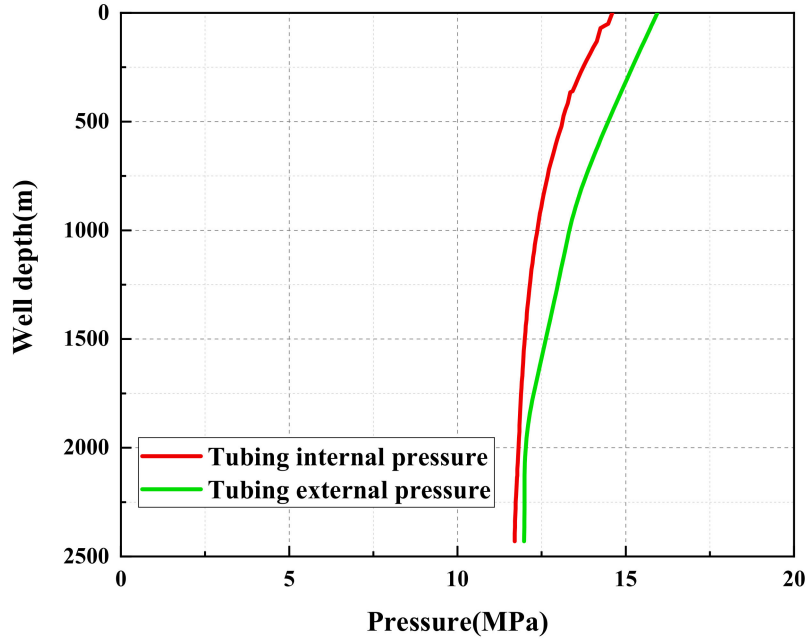


Figure 9. Pressure distribution of the integrated injection-production string.

As shown in Figure 8, the temperature inside the string decreases from 340 °C at the wellhead to 322.7 °C at the bottom of the well, and the annular temperature decreases from 55 °C at the wellhead to 38.5 °C (well depth 474 m) and, subsequently, increases to 60.7 °C at the bottom of the well.

As shown in Figure 9, the pressure inside and outside the string decreases with well depth. The pressure inside the string decreases from 14.6 MPa to 11.7 MPa, and the annular pressure decreases from 15.9 MPa at the wellhead to 12.0 MPa at the bottom of the well.

3.2.3. Strength Check Analysis

According to the above model, the calculated axial force distribution and strength check results of the string are shown in Figures 10 and 11, respectively.

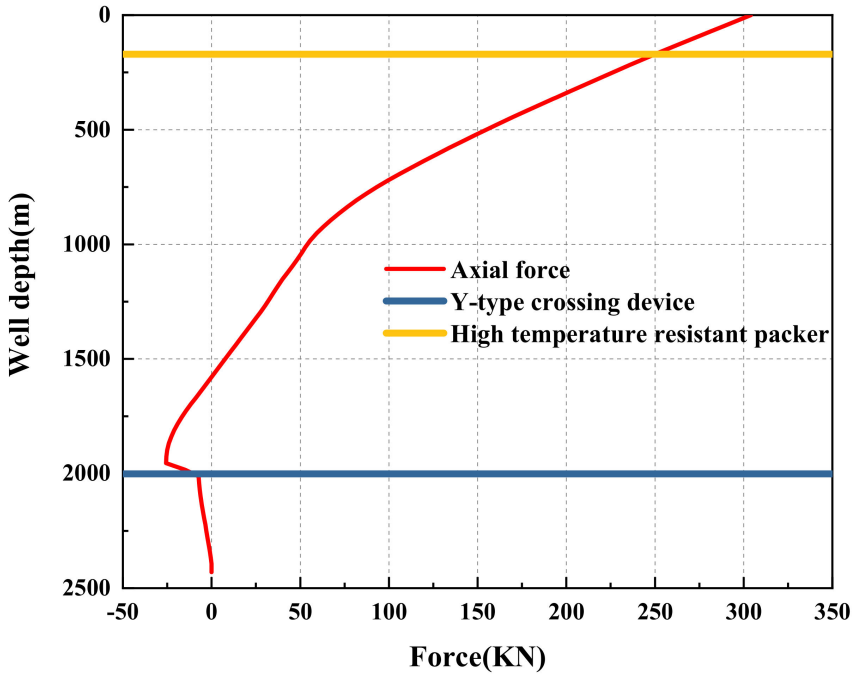


Figure 10. Axial force distribution of integrated injection-production string.

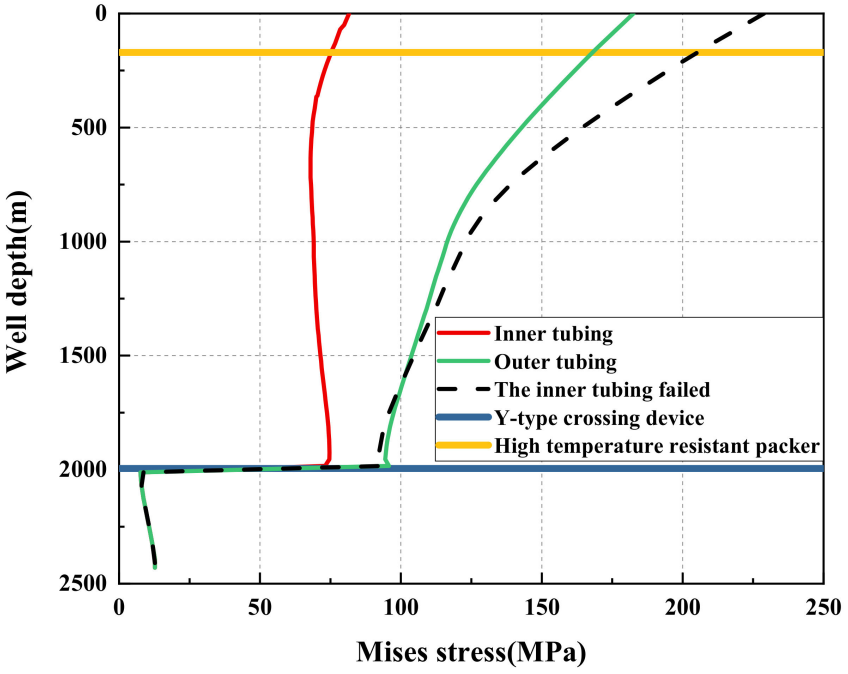


Figure 11. The von-Mises stress distribution of integrated injection-production string.

As shown in Figure 10, the axial force on the string gradually decreases from 304.1 KN to 25.1 KN (well depth of 1968 m), and then decreases to 0 KN (bottom hole). Due to the temperature effect caused by the temperature difference between the inside and outside of the string, the theoretical elongation of the string is 8.02 m. According to the compensation distance of the packer, the actual elongation of the string is 5.02 m.

As shown in Figure 11, the von-Mises stress of the outer layer of the string decreases from 182.5 MPa at the wellhead to 95.5 MPa (the upper part of the Y-type device). The von-Mises stress of the inner layer of the string decreases from 81.6 MPa to 75.5 MPa (the upper part of the Y-type device). When considering the failure of the inner tubing, the von-Mises stress at the wellhead increased to 228.9 MPa. The initial yield strength of the

string is 758.4 MPa. It could be concluded that the von-Mises stress did not achieve the yield strength. Therefore, the string does not fail due to strength issues.

3.2.4. Fatigue Damage

According to the above model, the calculated fatigue damage distribution of the integrated injection-production string is shown in Figure 12.

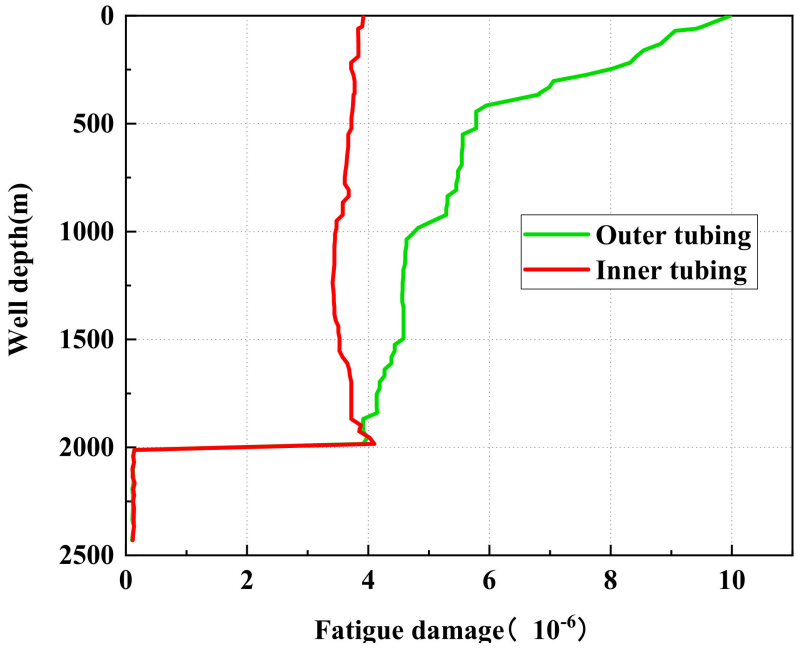


Figure 12. Fatigue damage distribution of the string.

As shown in Figure 11, with an increase in well depth, the fatigue damage of the string decreases. The maximum fatigue damage of the outer layer of the string is 9.9×10^{-6} at the wellhead. The maximum fatigue damage of the inner layer of the string is 4.2×10^{-6} near the Y-shaped device. However, the fatigue damage of the whole string is small, about 10^7. Thus, the probability of the pure mechanical fatigue failure of the string is low under the gas injection condition.

3.2.5. Corrosion Mechanism Analysis

The corrosion products are Fe_3O_4-dominated iron oxide and SiO_2 silt, and there is also a small amount of chlorine from water. Therefore, the corrosion type of the string is determined to be oxygen corrosion in a high-temperature and high-pressure water vapor environment.

3.2.6. Life Prediction after Corrosion

According to the corrosion standard [40], since the integrated injection-production string is in a complex environment, such as HTHP, for a long time, the corrosion grade is set as C5, and the sensitivity analysis of the corrosion rate is carried out. According to the above model, the calculated corrosion life distribution of the integrated injection-production string is shown in Figures 13 and 14.

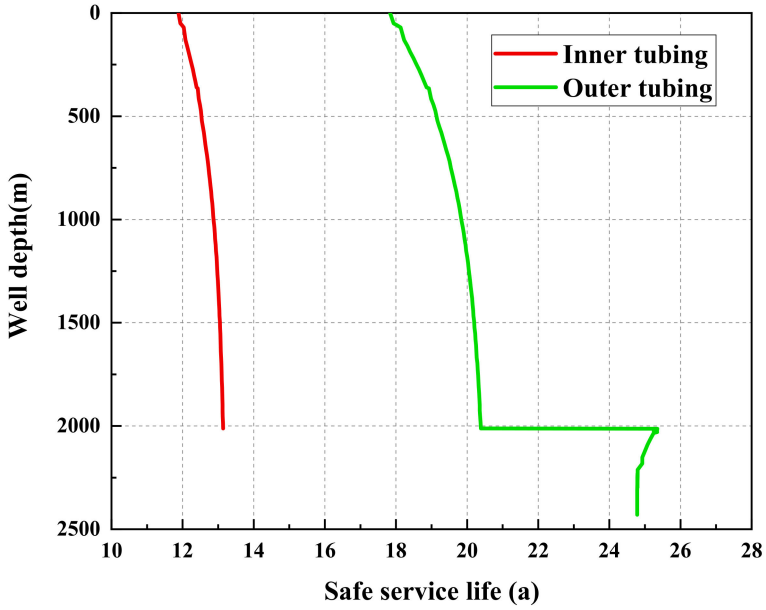


Figure 13. Corrosion life distribution of insulated tubing under uniform corrosion.

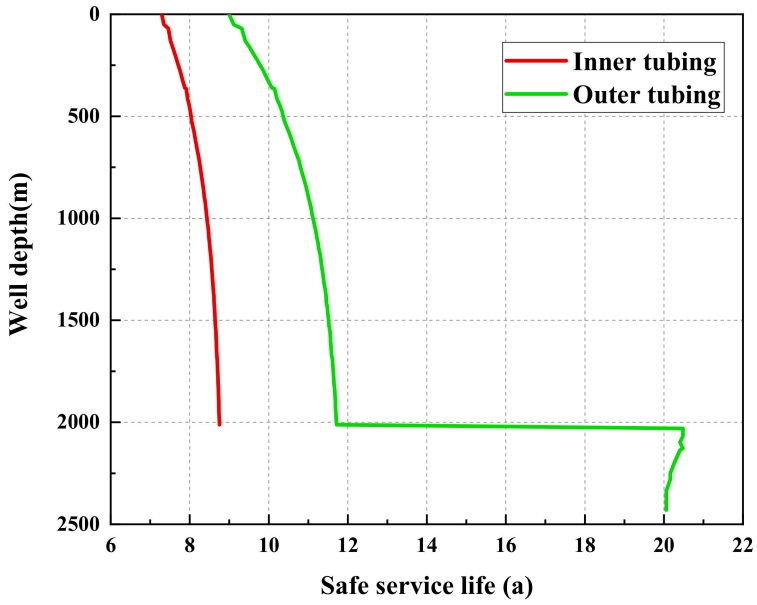


Figure 14. Corrosion life distribution of the string.

As shown in Figure 13, the corrosion life of the inner and outer layers of the string increases with well depth. The inner layer of the string increases from 12 years to 13.2 years. Since the length of the string is only 2000 m, there is a small length of single-layer string connected to the lower end of the outer layer of the string from 2000 m to 2430 m. Therefore, the corrosion life of the outer layer of the string increases from 17.8 years to 20.4 years, and then there is a sudden increase to 25.3 years. Finally, the corrosion life gradually decreases to 24.8 years due to the increase in internal and external pressure. The lowest corrosion life of the inner and outer layers of the string appears at the wellhead.

As shown in Figure 14, the corrosion life of the inner and outer layers of the string under local corrosion increases with well depth. The corrosion life of the inner layer of the string increases from 7.3 years to 8.7 years, and the corrosion life of the outer layer of the string increases from 9 years to 11.7 years; then, there is a sudden increase to 20.6 years. Finally, the corrosion life gradually decreases to 20.1 years. The lowest corrosion life for the inner and outer layers of the string appears at the wellhead.

3.2.7. Influence of Stress Concentration Coefficient

Sensitivity analysis of stress concentration coefficient under local corrosion was carried out, and the results are shown in Figures 14 and 15.

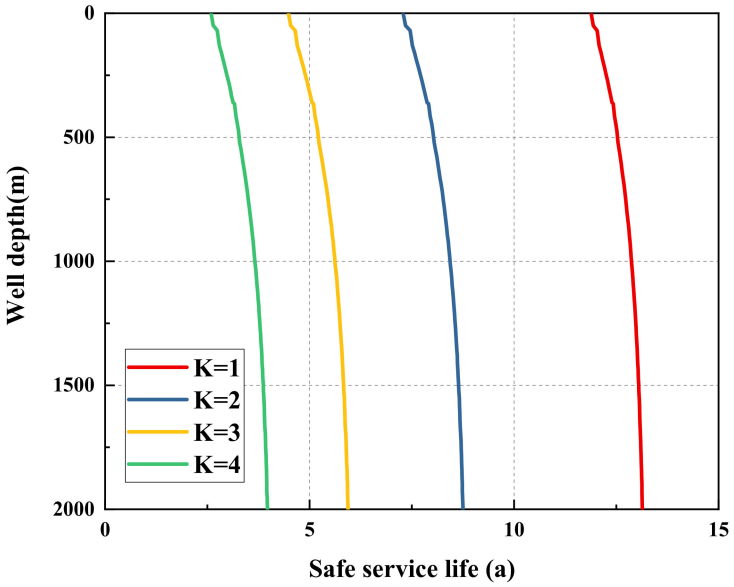


Figure 15. Influence of the stress concentration coefficient on the corrosion life of the inner layer of the string.

As shown in Figures 15 and 16, the lowest corrosion life of the string is located at the wellhead. When K = 1 to 4, the inner layer of the string decreases from 11.9 years to 2.6 years, and the outer layer of the string decreases from 17.8 years to 0.9 years. So, a conclusion can be drawn that the corrosion life of the string will decrease with an increase in the stress concentration coefficient.

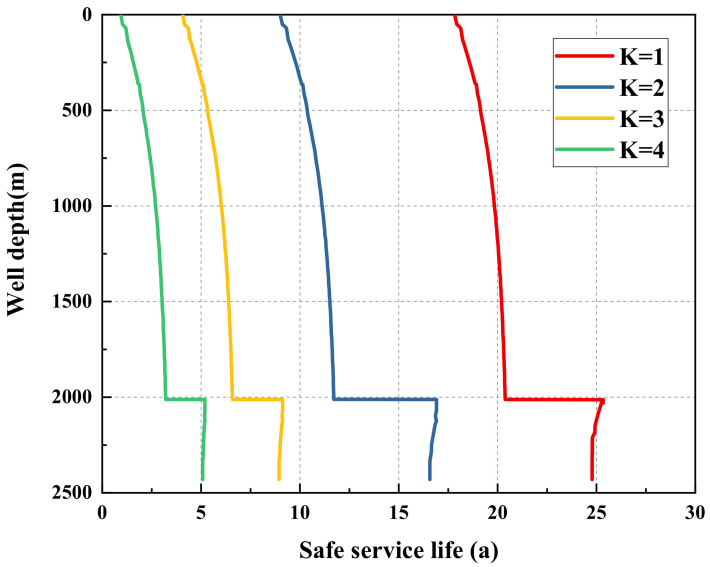


Figure 16. Influence of the stress concentration coefficient on the corrosion life of the outer layer of the string.

3.2.8. Influence of Corrosion Rate

The influence of corrosion rate on the service life is shown in Figures 17 and 18.

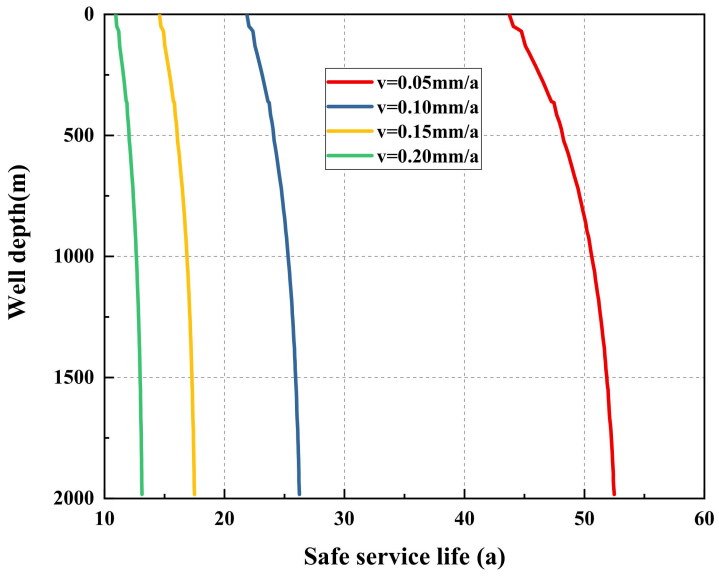


Figure 17. Influence of corrosion rate on the corrosion life of the inner layer of the string.

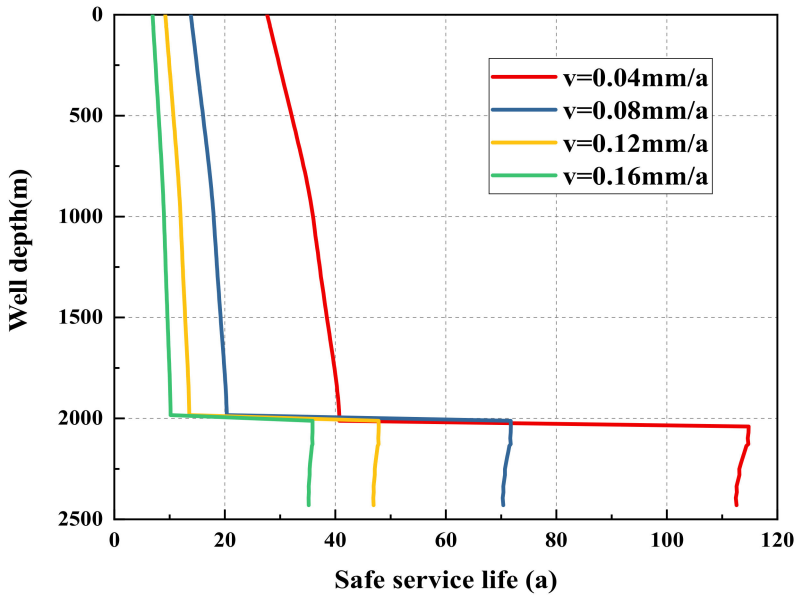


Figure 18. Influence of corrosion rate on the corrosion life of the outer layer of the string.

As shown in Figures 17 and 18, the smallest corrosion life for the string is also located at the wellhead. When the corrosion rate of the inner string is 0.05–0.20 mm/a and that of the outer string is 0.04–0.16 mm/a, the service life of the inner string reduces from 8.7 years to 5.3 years, while the same for the outer string reduces from 13.5 years to 5.4 years. As can be seen from Figures 12–17, the lowest corrosion life is located at the wellhead. Thus, the corrosion-resistant strings should be used in this section.

4. Conclusions

1. In this paper, the temperature, pressure, and strength check of an integrated injection-production string were analyzed. It is concluded that the von-Mises stress did not achieve the required yield strength, which means that the string does not fail due to strength issues;
2. Vibration fatigue is not the main reason for the failure of the string under the gas injection condition;

3. The oxygen-based corrosion of the string under the condition of hot steam is the main reason leading to the corrosion of the integrated injection-production string. After corrosion, the strength of the string decreases, and strength failure will occur under the action of an external load.

Author Contributions: Conceptualization, W.Z.; validation, W.Z.; formal analysis, W.Z.; investigation, C.W.; resources, J.B. and Y.L.; data curation, W.Z.; writing—original draft, W.Z.; supervision, D.G. and Y.L.; project administration, D.G., and Y.L. All authors have read and agreed to the published version of the manuscript.

Funding: This research received no external funding.

Data Availability Statement: Not applicable.

Acknowledgments: The authors would like to thank the reviewers for their many constructive suggestions and comments that helped improve the quality of the paper.

Conflicts of Interest: The authors declare no conflict of interest.

References

1. Dong, X.H.; Liu, H.Q.; Chen, Z.X.; Wu, K.L.; Lu, N.; Zhang, Q.C. Enhanced Oil Recovery Techniques for Heavy Oil and Oilsands Reservoirs after Steam Injection. *Appl. Energy* **2019**, *239*, 1190–1211. [CrossRef]
2. Li, Q.; Han, Y.; Liu, X.; Ansari, U.; Cheng, Y.; Yan, C. Hydrate as A By-product in CO_2 Leakage during the Long-term Sub-seabed Sequestration and Its Role in Preventing Further Leakage. *Environ. Sci. Pollut. Res. Int.* **2022**, *29*, 77737–77754. [CrossRef] [PubMed]
3. Li, Q.; Wang, F.L.; Wang, Y.L.; Zhou, C.; Chen, J.S.; Kobina, F.; Miao, R.F.; Su, Y.J.; Zhang, J.Y. Effect of Reservoir Characteristics and Chemicals on Fltration Property of Water-based Drilling Fluid in Unconventional Reservoir and Mechanism Disclosure. *Environ. Sci. Pollut. Res. Int.* **2023**. [CrossRef]
4. Cullender, M.H.; Smith, R.V. Practical Solution of Gas-Flow Equations for Wells and Pipelines with Large Temperature Gradients. *Trans. AIME* **1956**, *205*, 281–287. [CrossRef]
5. Ramey, H.J. Wellbore Heat Transmission. *J. Pet. Technol.* **1962**, *14*, 427–435. [CrossRef]
6. Wang, M.K. Quantitative Calculation of Wellbore Heat Transmission for Steam Injection Wells. *J. Univ. Pet.* **1994**, *18*, 77–82.
7. Mao, W.; Liang, Z. Coupling Analysis of The Pressure and Temperature in Gas Well Borehole. *Nat. Gas Ind.* **1999**, *19*, 66–69.
8. Zhang, Y.K.; Cai, B.; Liu, Y. Modifications to The Calculation Method of Flowing Pressure Gradient in Gas Well Tubing. *Nat. Gas Ind.* **2007**, *27*, 89–91, 156.
9. Shi, X.L.; Gao, D.L.; Wang, Y.B. Predictive Analysis on Borehole Temperature and Pressure of HTHP Gas Wells Considering Coupling Effect. *Oil Drill. Prod. Technol.* **2018**, *40*, 541–546. [CrossRef]
10. Cao, L.H.; Sun, J.S.; Zhang, B.; Lu, N.; Xu, Y.Q. Sensitivity Analysis of The Temperature Profile Changing Law in The Production String of A High-pressure High-temperature Gas Well Considering the Coupling Relation among The Gas Flow Friction, Gas Properties, Temperature, and Pressure. *Front. Phys.* **2022**. [CrossRef]
11. Cao, L.H.; Sun, J.S.; Liu, J.Y.; Liu, J.Q. Experiment and Application of Wax Deposition in Dabei Deep Condensate Gas Wells with High Pressure. *Energies* **2022**, *15*, 6200. [CrossRef]
12. Johancsik, C.A.; Friesen, D.B.; Dawson, R. Torque and Drag in Directional Wells-Prediction and Measurement. *J. Pet. Technol.* **1984**, *36*, 987–992. [CrossRef]
13. Mitchell, R.F.; Samuel, R. How Good Is the Torque/Drag Model? *SPE Drill. Complet.* **2009**, *24*, 62–71. [CrossRef]
14. Mayouf, M.; Hadjadj, A. A Stiff-String Model for Torque and Drag Analysis in Directional Wells. *Arab. J. Sci. Eng.* **2022**, *47*, 12089–12102. [CrossRef]
15. Wang, Y.B.; Shi, X.L.; Gao, D.L.; Zhang, J.S.; Chen, J.J. Failure Analysis of Completion Test String for Deep High-temperature and High-pressure Gas Well: A Case Study on A Well in Shunnan Area. *Oil Drill. Prod. Technol.* **2022**, *44*, 302–308. [CrossRef]
16. Semler, C.; Li, G.X.; Paidoussis, M.P. The Non-linear Equations of Motion of Pipes Conveying Fluid. *J. Sound Vib.* **1994**, *169*, 577–599. [CrossRef]
17. Ding, J.D.; Lian, Z.H.; Ding, Y.R.; Zhang, Q.; Liu, L.W. Simulated Vibration Test and Vibration Law Analysis of Injection Pipe String in Gas Storage. *Pet. Tubul. Goods Instrum.* **2019**, *5*, 30–34. [CrossRef]
18. Manson, S.S. Interfaces between Fatigue, Creep, and Fracture. *Int. J. Fract. Mech.* **1966**, *2*, 327–363. [CrossRef]
19. Neuber, H. Theory of Stress Concentration for Shear-Strained Prismatical Bodies with Arbitrary Nonlinear Stress-Strain Law. *J. Appl. Mech.* **1961**, *28*, 544–550. [CrossRef]
20. Chen, N.Z.; Wang, G.; Soares, C.G. Palmgren–Miner's Rule and Fracture Mechanics-based Inspection Planning. *Eng. Fract. Mech.* **2011**, *78*, 3166–3182. [CrossRef]

21. Liu, G.J.; Wang, D.H.; Hu, Z.Y. Application of The Rain-flow Counting Method in Fatigue. In Proceedings of the 2016 2nd International Conference on Electronics, Network and Computer Engineering (ICENCE 2016), Yinchuan, China, 13–14 August 2016; pp. 247–251.
22. Liu, J.; Li, J.; Guo, X.Q.; Wei, A.C.; Huang, L.; Wang, G.R. Fatigue Test and Fatigue Life Analysis of Tubing String in High-yield Curved Well. *China Pet. Mach.* **2021**, *49*, 86–95. [CrossRef]
23. Song, J.S.; Bowen, J. The Internal pressure capacity of crescent-shaped wear casing. In Proceedings of the IADC/SPE 23902 Drilling Conference, New Orleans, LA, USA, 15–21 February 1992.
24. Sun, K.; Guo, B.Y. Simple formula for calculating strength degradation of well casings and pipelines due to corrosion pitting. In Proceedings of the Asia Pacific Oil and Gas Conference and Exhibition, Perth, Australia, 18–20 October 2004.
25. Wu, J.; Chevron, T. Casing burst strength after casing wear. In Proceedings of the SPE 94304, SPE Production Operations Symposium, Oklahoma City, OK, USA, 17–19 April 2005.
26. Mu, L.J.; Zhang, J.; Zhao, W.Z.; Jing, L.J.; Chen, L. Strength and Service Life of Casing under Uniform Corrosion. *Corros. Prot. Petrochem.* **2010**, *27*, 10–13.
27. Yuan, S.P.; Luo, H.; Cai, P.; Mao, L.; Liu, X.H. Numerical Simulation of Corrosion and Wear of Oil and Gas Well Casing in Bohai Oilfield. *Tianjin Sci. Technol.* **2019**, *46*, 29–36. [CrossRef]
28. Xu, G.X.; Xie, R.J.; Wu, Y.; Yin, Q.S. Prediction Method of Residual Strength of Casing with Different Corrosion Defects. *China Pet. Mach.* **2019**, *47*, 122–127. [CrossRef]
29. Hasan, A.R.; Wang, X.; Kabir, C.S. A Transient wellbore/reservoir model for testing gas wells in high-temperature reservoir. Part II. Field Application. In Proceedings of the PE Annual Technical Conference and Exhibition, New Orleans, LA, USA, 24–27 September 1994.
30. Palatz. *Thermal Oil Recovery*; Wang, M.K., Ed.; Petroleum Industry Press: Beijing, China, 1989; pp. 37–65.
31. Li, Q.D.; Xie, G.P.; Zhang, J. Calculation Analysis of Amount of Deformation of Free Movement Packer String—The Fourth Discussion of Force Analysis System of Packer String. *Drill. Prod. Technol.* **2002**, *1*, 60–64.
32. Wang, B. Mechanical Analysis and Safety Evaluation of High Temperature and High Pressure Completion String. Master's Thesis, Southwest Petroleum University, Sichuan, China, 2014.
33. Hill, R. *The Mathematical Theory of Plasticity*; Oxford University Press: Oxford, UK, 1998; Volume 11.
34. Guo, Y.Q.; Long, J.Y. The Rain Flow Counting Method and Its Statistical Processing Program Were Improved. *J. Mech. Strength* **1987**, 45–48. [CrossRef]
35. Wang, H.W.; Xing, B.; Luo, H.Y. Rain Flow Counting Method and Its Application in Fatigue Life Estimation. *Min. Process. Equip.* **2006**, *34*, 95–97.
36. Xu, H. *Fatigue Strength*; Higher Education Press: Beijing, China, 1988.
37. Jiang, Z.G.; Zhang, J.M.; Liu, S.Q.; Han, X.K.; Liu, Z.B.; Xing, S.C. Development and Application of Goodman Fatigue Limit Diagram Program. *Tract. Farm Transp.* **2022**, *49*, 43–46.
38. Yan, Y.F.; Shao, B.; Tian, W.; Yan, X.Z. The Fatigue Reliability Analysis of Injection-production Casing in the Underground Gas Storage Based on Multi-level Loading Experiment. *China Meas. Test* **2015**, *41*, 110–114. [CrossRef]
39. Gutman. *Mechanical Chemistry and Corrosion Protection of Metals*; Science Press: Beijing, China, 1989; Volume 36.
40. *ISO 9223:2012*; Corrosion of Metals and Alloys—Corrosivity of Atmospheres—Classification, Determination and Estimation. International Standard ISO: Geneva, Switzerland, 2012.

Disclaimer/Publisher's Note: The statements, opinions and data contained in all publications are solely those of the individual author(s) and contributor(s) and not of MDPI and/or the editor(s). MDPI and/or the editor(s) disclaim responsibility for any injury to people or property resulting from any ideas, methods, instructions or products referred to in the content.